Optics Letters

716 nm deep-red passively Q-switched Pr:ZBLAN all-fiber laser using a carbon-nanotube saturable absorber

Wensong Li,[1] Tuanjie Du,[1] Jinglong Lan,[1] Changlei Guo,[1] Yongjie Cheng,[1] Huiying Xu,[1] Chunhui Zhu,[2] Fengqiu Wang,[2,4] Zhengqian Luo,[1,3] and Zhiping Cai[1,*]

[1]Department of Electronic Engineering, School of Information Science and Engineering, Xiamen University, Xiamen 361005, China
[2]School of Electronic Science and Engineering, Collaborative Innovation Center of Advanced Microstructures, Nanjing University, Nanjing 210023, China
[3]Shenzhen Research Institute of Xiamen University, Shenzhen 518057, China
[4]e-mail: fwang@nju.edu.cn
*Corresponding author: zpcai@xmu.edu.cn

Received 7 November 2016; revised 15 January 2017; accepted 16 January 2017; posted 17 January 2017 (Doc. ID 280255); published 3 February 2017

We experimentally demonstrated a compact single-wall carbon-nanotube (SWNT)-based deep-red passively Q-switched Pr^{3+}-doped ZBLAN all-fiber laser operating at 716 nm. A free-standing SWNT/polyvinyl alcohol composite film embedded between a pair of fiber connectors was employed as a saturable absorber (SA). The deep-red Q-switched operation is attributed to the combination of implementing a pair of fiber end-facet mirrors to achieve the linear laser resonator and incorporating a SWNT-SA into the cavity as a Q-switcher. Stable short-pulse generation with a duration of 2.3 μs was realized. When gradually increasing the incident pump power, the pulse repetition rate can be linearly tuned from 32.6 to 86.5 kHz, corresponding to a maximum average output power of 1.5 mW and the highest single-pulse energy of 18.3 nJ. To the best of our knowledge, this is the first demonstration of SWNT-based SA for a Q-switched laser at a deep-red wavelength ~716 nm.

OCIS codes: (140.3510) Lasers, fiber; (140.7300) Visible lasers; (140.3540) Lasers, Q-switched; (160.4236) Nanomaterials.

https://doi.org/10.1364/OL.42.000671

All-fiber laser sources have attracted considerable research interest owing to their compact, convenient, and cost-effective designs. Compared with continuous wave (CW) ones, pulsed lasers (i.e., Q-switched/mode-locked operation) can achieve high peak power and release large amounts of energy within a short temporal duration, thus reinforcing their practical applications. To date, however, operation wavelengths for short-pulse lasers have been essentially limited in the near-infrared region. In order to open up new application fields, there is a growing interest to achieve short-pulse generation for shorter wavelengths than those of the communication window. For example, using pulsed all-fiber lasers at the visible spectral range proves useful for a number of applications fields, such as biology and microscopy. In particular, a deep-red wavelength at around 700 nm, which is characterized by the absence of strong absorption by water, blood, and hemoglobin, holds a lower optical scattering within the dermis [1–3]. Such a feature is useful for photo-medicine and bio-photonic applications that benefit from a large penetration depth into the tissue, such as fluorescence imaging, photodynamic therapy, and stimulated emission depletion microscopy [4–6]. In the past two dades, the Pr^{3+}-doped ZrF_4-BaF_2-LaF_3-AlF_3-NaF (Pr:ZBLAN) fiber had been commonly employed as the active media to realize visible fiber lasers [7,8]. Pulsed generation based on a passive format enabled by saturable absorber (SA) is generally more desirable due to its low cost and free maintenance in comparison with the active one, which usually needs an externally driven modulator. However, to the best of our knowledge, deep-red pulsed all-fiber laser operation has not been achieved thus far.

At present, nanomaterial-based SAs have been extensively used for all-fiber pulsed laser operation, including single-wall carbon nanotubes (SWNTs) [9–12], graphene [13–15], transition-metal dichalcogenides (TMDs) [16,17]. Very recently, we have demonstrated visible passively Q-switched all-fiber lasers with TMD-based SAs, e.g., red-light [18] and orange-light [19]. As the very first nanomaterial-based SA, SWNTs have been widely believed to be a narrow bandwidth SA, where the customization of operation wavelengths is achieved through the control of the diameter and chirality of constituent nanotubes so that an absorption resonance overlaps with the desired laser wavelength [20,21]. Utilizing such a design guideline, SWNT-based Q-switched/mode-locked lasers have been demonstrated mainly across the 1–2 μm spectral regions [22–26]. It is not fully clear whether SWNTs can be applied as effective SAs operating at visible wavelengths. Recently, Xu *et al.* combined Z-scan and degenerate pump-probe techniques to

reveal broadband saturable absorption properties of SWNTs; it is experimentally confirmed that nonlinear absorption of SWNTs extends into the visible range [27].

In this Letter, we experimentally demonstrate a compact deep-red passively Q-switched all-fiber laser based on SWNT-SA. The all-fiber laser cavity was made up of a fiber-coupled 445 nm pump source, a Pr:ZBLAN active fiber, and a pair of deep-red highly reflective fiber mirrors. The SA made of SWNT/polyvinyl alcohol (PVA) composite can be inserted into a fiber connector, enabling a compact laser architecture with good reproducibility. Stable passive Q-switching operation at 716 nm was successfully achieved. Such an all-fiber laser has a tunable pulse repetition rate ranging from 32.6 to 86.5 kHz, a narrow pulse duration of 2.3 μs, and a maximum average output power of 1.5 mW.

In our experiment, the SWNT sample was prepared by the electric arc-discharge method [23,27]. A SWNT/PVA film was fabricated by evaporating the SWNT polymer composite solution to dryness; then we cut the film into small pieces for practical use [18]. Optical transmittance of the SWNT/PVA film and pure PVA film, as shown in Fig. 1(a), was measured by an UV/VIS spectrometer (Perkin Elmer, Lambda750). It is observed that the transmission increases gradually from 41.64% to 48.87%, with a wavelength between 600 and 800 nm, a range that corresponds to the metallic M_{11} excitonic band [27,28], which indicates its visible operation regime. Note that pure PVA has a higher transmission around 700 nm. Figure 1(b) shows the transition absorption curve of the SWNT/PVA film for a 700 nm excitation wavelength, which is performed by a degenerate pump-probe experiment [18,27]. The experimental measurement can be well fitted by a mono-exponential decay with a time constant of ~1 ps [29], attributable to nonlinear photoexcitation that mainly originates from metallic tube transitions. The SWNT sample has a saturable absorption of 19% at 700 nm, i.e., the ratio of saturable/non-saturable absorption is estimated to be 0.23 [27]. This result indicates the ultrafast saturable absorption of the as-prepared SWNT sample at 700 nm and confirms that the SWNT is very promising for pulse generation in shorter visible region.

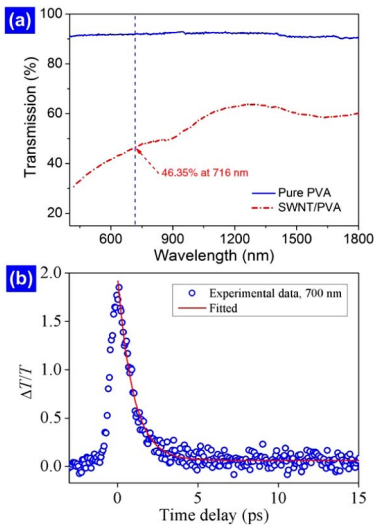

Fig. 1. (a) Optical transmission spectra of the as-prepared SWNT/PVA film and pure PVA film. The vertical dashed line denotes the laser operation wavelength at 716 nm. (b) Relative change of transmission for a 700 nm excitation wavelength.

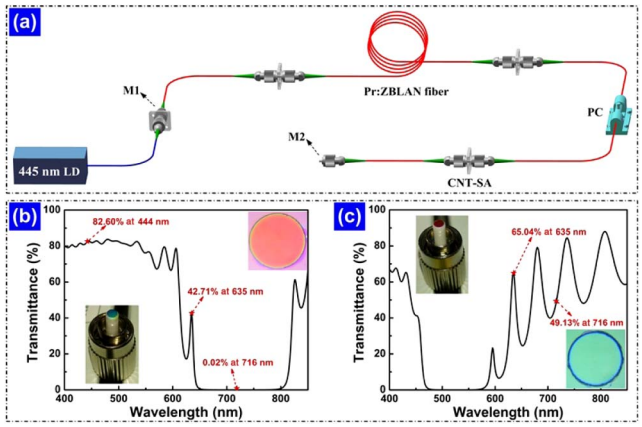

Fig. 2. (a) Experimental setup of the deep-red Q-switched all-fiber laser. (b, c) Optical transmission spectra of the fiber end-facet mirrors as the input M1 and output M2 mirrors, respectively. Insets: photographs and microscopic images of M1 and M2.

Figure 2 specifically illustrates the experimental arrangement. As shown in Fig. 2(a), the proposed compact SWNT-based passively Q-switched deep-red all-fiber laser, with a cavity length of about 4.2 m, simply consists of a 445 nm GaN LD, a Pr:ZBLAN fiber, a pair of fiber end-facet mirrors, and a fiber-compatible SWNT Q-switcher. A homemade ~0.5 W, 445 nm fiber-coupled diode laser (core/cladding, 5.8/125 μm; NA, 0.13) was used as the pump source. We employed a 0.9 m long Pr:ZBLAN fiber (core/cladding, 6/125 μm; NA, 0.15; Pr^{3+}, 1000 ppm, absorption coefficients of ~18.8 dB/m at 445 nm, and less than 0.1 dB/m at 716 nm) as the gain medium, which is slightly hygroscopic insensitive. The all-fiber linear cavity for deep-red laser oscillation was constructed by the homemade fiber end-facet mirrors (M1 and M2). Both mirrors were fabricated by coating SiO_2/Ta_2O_5 dielectric film onto fiber ferrules of the SMF 1060-XP using a plasma sputter deposition system (SCT-S500, System Control Technologies, Inc.). As displayed in Fig. 2(b), we measured the transmission spectrum of the input mirror M1, with a high transmittance of 82.60% at 445 nm (i.e., 82.60% at 445 nm), as well as a high reflectivity of 99.98% at 716 nm (i.e., 0.02% at 716 nm). As seen from Fig. 2(c), the transmission spectrum of the output mirror M2 was also manifested. It had a transmittance of 49.13% at a 716 nm wavelength. It should be noted that the emission peak at 716 nm of the used Pr:ZBLAN fiber excited by a 445 nm LD is the relative lowest; however, there is the strongest optical gain at around 635 nm, as measured in our previous report [18]. Herein, owing to the cavity mirrors M1 and M2, designed with a transmittance of 42.71% and 65.04% at 635 nm, respectively, the gain competition in the Pr:ZBLAN fiber finally leads to the 716 nm lasing only, assuming that the polarization controller (PC) is properly adjusted. The free-standing SWNT/PVA film was sandwiched between two fiber ferrules to construct a fiber-compatible SWNT SA. Then, the SWNT-SA was incorporated into the laser cavity, acting as a Q-switcher.

The output characteristics of the Q-switched laser were recorded by a photodetector (Thorlabs, DET10A) together with

a Tektronix TDS4054B digital oscilloscope (500 MHz bandwidth, 2.5 Gs/s sampling rate) and a radio-frequency (RF) spectrum analyzer (Gwinstek GSP-930). The optical spectra of the laser output were monitored by a 300–1200 nm optical spectrum analyzer (OSA; HR-4000, Ocean Optics), and a 600–1700 nm OSA (HP 70951B). The average output power was measured by a power meter (Coherent PM3).

In our experiment, the deep-red CW all-fiber laser was initiated at the incident pump power (P_P) of ~110 mW because of separating the SWNT-SA from the laser cavity. At the moment, whether changing the P_P or manipulating the PC, only CW lasing at 716 nm was observed in the laser cavity identified by the oscilloscope and the OSA due to the lack of a modulation factor, which excluded the possibility of self-pulsing. Here, we measured a CW laser output power of 10 mW at the P_P of 260 mW. In contrast, once the SWNT-SA was integrated into the cavity, stable self-started Q-switched operation launched when the P_P was over 130 mW. The insertion loss of the SWNT-SA was calculated to be about 0.72 dB. As summarized in Fig. 3, we give the typical characteristics of the deep-red Q-switched all-fiber laser. Figure 3(a) systematically depicts the evolutions of the pulse trains under different incident pump powers. The pulse repetition rate becomes higher and higher, along with the increased P_P, which indicates a typical passively Q-switched operation [30]. At the P_P of 167.8 mW, a single-pulse envelope with the duration of 4.1 μs is shown in Fig. 3(b). It has a symmetric Gaussian-like intensity profile. The output optical spectrum of the Q-switched operation at the P_P of 219.1 mW was measured and normalized, as plotted in Fig. 3(c). In addition, the inset of Fig. 3(c) gives a close look at 716 nm with a full width at half-maximum (FWHM) of 0.83 nm. Meanwhile, the corresponding optical spectrum of the CW emission state at the P_P of 219.1 mW is also displayed in the inset of Fig. 3(c) as a comparison, from which we can infer that the FWHM of CW output at 716 nm was about 1.54 nm. It is the increased intra-cavity loss that, originating from the incorporation of SWNT-SA into the cavity, contributes to the single-peak lasing at 716 nm in the Q-switched regime.

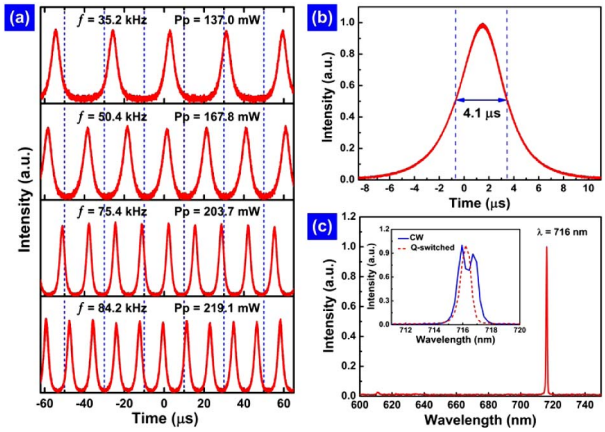

Fig. 3. Characteristics of the deep-red Q-switched all-fiber laser. (a) Evolutions of the Q-switching pulse trains under different incident pump powers at P_P=137.0mW, P_P=167.8mW, P_P = 203.7 mW, and P_P = 219.1 mW. (b) Single-pulse profile at P_P = 167.8 mW. (c) Output optical spectrum at P_P = 219.1 mW. Inset: optical spectra of CW and Q-switched laser.

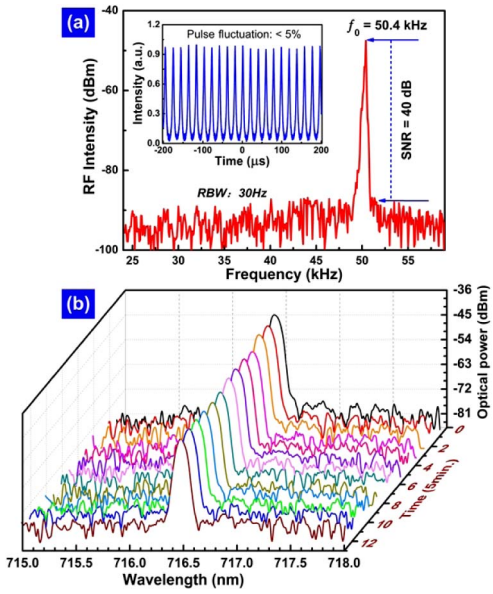

Fig. 4. (a) RF spectrum of the deep-red Q-switched all-fiber laser at the P_P of 167.8 mW. Inset: typical pulse train at the repetition rate of 50.4 kHz. (b) Repeated output optical spectra recorded under different times.

To evaluate the stability of the passively Q-switched deep-red laser oscillation, we measured the RF spectrum and the output optical spectra every 5 minutes over an hour under fixed experimental condition (e.g., P_P = 167.8 mW), as presented in Fig. 4. One can see from the Fig. 4(a), the RF signal-to-noise ratio is nearly 40 dB, which is comparable to those passively Q-switched visible or near-IR fiber lasers by 2D nanomaterials as SAs [18,31]. Correspondingly, the inset of Fig. 3(a) shows the real-time oscilloscope trace with a pulse repetition rate of 50.4 kHz. It has a pulse-intensity fluctuation as low as 5%. Furthermore, Fig. 4(b) exhibits the repeated output spectra scanned under different times. Neither the central wavelength movement nor the new wavelength component was observed during the measurement, illustrating excellent repeatability and long-term stability. Such results clearly confirm that the SWNT-based deep-red passively Q-switched all-fiber laser at 716 nm is stable and could be suitable for practical application.

As shown in Fig. 5, we performed the Q-switched pulse parameter variation with the P_P. Figure 5(a) draws the relationship curves of the output power and pulse energy along with the P_P. The output power increases linearly with a maximum value of 1.5 mW. Nevertheless, the pulse energy linearly boosts in the case of low P_P, after the P_P exceeds 173 mW; the pulse energy becomes saturated obviously, most probably due to the

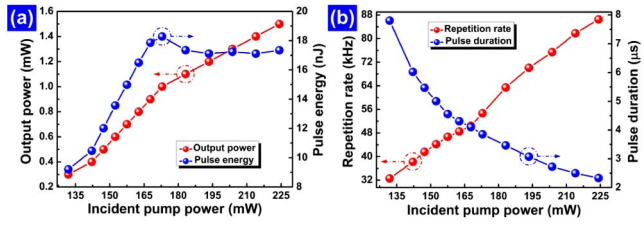

Fig. 5. (a) Output power and pulse energy. (b) Repetition rate and pulse duration as a function of the P_P.

thermal accumulation of the SWNT-SA in the case of high P_P, inducing the bleaching effects [32]. Here, the obtained maximum pulse energy is 18.3 nJ at the P_P of 173 mW, comparable to those ever reported SWNT-based Q-switched all-fiber lasers [25,26,33,34]. Figure 5(b) gives the dependence of the repetition rate and pulse duration on the P_P. It is seen that the repetition rate increased almost linearly from 32.6 to 86.5 kHz as the variation of the P_P, whereas the pulse duration decreased from 7.8 to 2.3 μs. The pump rate for the upper laser level increases with increasing the P_P and causes the reduction of the pulse duration and the increase of the repetition rate [23,25]. As the P_P went beyond 224 mW, the Q-switched operation became unstable where strong pulse fluctuation appeared, which was attributed to the thermal damage of the SWNT-SA induced by optical power. Here, a higher P_P would lead to the permanent disappearance of the Q-switched pulse, so we measured the damage threshold of the SWNT-SA, which was ~230 mW. Further works need to be addressed for the optimized performance of the deep-red passively Q-switched all-fiber laser, i.e., shorter pulse duration and higher pulse energy, or achieving the visible mode-locked all-fiber lasers, such as perfecting the cavity designs [35,36], improving the modulation depth of SWNT-SA, and optimizing the dispersion management (e.g., short gain medium, photonic crystal fiber) [37].

In conclusion, we experimentally achieved a compact deep-red passively Q-switched all-fiber laser using SWNT-SA. A pair of fiber end-facet mirrors constructed a linear all-fiber resonant cavity and a Pr:ZBLAN active fiber pumped by a fiber-coupled 445 nm LD provided the laser gain. Stable pulse generation from the deep-red Q-switched all-fiber laser was characterized by a tunable repetition rate of 32.6–86.5 kHz, a narrow pulse duration of 2.3 μs, and a maximum pulse energy of 18.3 nJ. To the best of our knowledge, this is the first demonstration of a SWNT-based pulsed all-fiber laser operating at a shorter wavelength of 716 nm. Such a result provides a promising approach to achieve compact, robust, cost-effective deep-red pulsed laser sources, and may introduce various applications in bio-photonics and photo-medicine.

Funding. National Natural Science Foundation of China (NSFC) (61275050, 61378025); Shenzhen Science and Technology Projects (JCYJ20160414160109018).

REFERENCES

1. J. A. Parrish, J. Invest. Dermatol. **77**, 45 (1981).
2. S. L. Jacques, Phys. Med. Biol. **58**, R37 (2013).
3. E. J. Saarinen, J. Lyytikäinen, S. Ranta, A. Rantamäki, A. Sirbu, V. Iakovlev, E. Kapon, and O. G. Okhotnikov, Opt. Lett. **40**, 4380 (2015).
4. M. Heilemann, S. van de Linde, M. Schuttpelz, R. Kasper, B. Seefeldt, A. Mukherjee, P. Tinnefeld, and M. Sauer, Angew. Chem. Int. Ed. **47**, 6172 (2008).
5. D. Wildanger, E. Rittweger, L. Kastrup, and S. W. Hell, Opt. Express **16**, 9614 (2008).
6. P. Agostinis, K. Berg, K. A. Cengel, T. H. Foster, A. W. Girotti, S. O. Gollnick, S. M. Hahn, M. R. Hamblin, A. Juzeniene, D. Kessel, M. Korbelik, J. Moan, P. Mroz, D. Nowis, J. Piette, B. C. Wilson, and J. Golab, CA-Cancer J. Clin. **61**, 250 (2011).
7. J. Y. Allain, M. Monerie, and H. Poignant, Electron. Lett. **27**, 189 (1991).
8. Y. Fujimoto, J. Nakanishi, T. Yamada, O. Ishii, and M. Yamazaki, Prog. Quantum Electron. **37**, 185 (2013).
9. Y.-C. Chen, N. R. Raravikar, L. S. Schadler, P. M. Ajayan, Y.-P. Zhao, T.-M. Lu, G.-C. Wang, and X.-C. Zhang, Appl. Phys. Lett. **81**, 975 (2002).
10. F. Wang, A. G. Rozhin, V. Scardaci, Z. Sun, F. Hennrich, I. H. White, W. I. Milne, and A. C. Ferrari, Nat. Nanotechnol. **3**, 738 (2008).
11. E. J. R. Kelleher, J. C. Travers, Z. P. Sun, A. G. Rozhin, A. C. Ferrari, S. V. Popov, and J. R. Taylor, Appl. Phys. Lett. **95**, 111108 (2009).
12. A. Martinez and Z. P. Sun, Nat. Photonics **7**, 842 (2013).
13. Q. Bao, H. Zhang, Y. Wang, Z. Ni, Y. Yan, Z. X. Shen, K. P. Loh, and D. Y. Tang, Adv. Funct. Mater. **19**, 3077 (2009).
14. H. Zhang, Q. Bao, D. Tang, L. Zhao, and K. Loh, Appl. Phys. Lett. **95**, 141103 (2009).
15. Y. Fujimoto, T. Suzuki, R. A. M. Ochante, T. Hirayama, M. Murakami, H. Shiraga, M. Yoshida, O. Ishii, and M. Yamazaki, Electron. Lett. **50**, 1470 (2014).
16. R. I. Woodward, E. J. R. Kelleher, R. C. T. Howe, G. Hu, F. Torrisi, T. Hasan, S. V. Popov, and J. R. Taylor, Opt. Express **22**, 31113 (2014).
17. Z. Luo, Y. Li, M. Zhong, Y. Huang, X. Wan, J. Peng, and J. Weng, Photon. Res. **3**, A79 (2015).
18. Z. Luo, D. Wu, B. Xu, H. Xu, Z. Cai, J. Peng, J. Weng, S. Xu, C. Zhu, F. Wang, Z. Sun, and H. Zhang, Nanoscale **8**, 1066 (2016).
19. W. Li, J. Peng, Y. Zhong, D. Wu, H. Lin, Y. Cheng, Z. Luo, J. Weng, H. Xu, and Z. Cai, Opt. Mater. Express **6**, 2031 (2016).
20. N. Hamada, S. Sawada, and A. Oshiyama, Phys. Rev. Lett. **68**, 1579 (1992).
21. H. Kataura, Y. Kumazawa, Y. Maniwa, Y. Ohtsuka, R. Sen, S. Suzuki, and Y. Achiba, Carbon **38**, 1691 (2000).
22. F. Wang, A. G. Rozhin, Z. Sun, V. Scardaci, R. V. Penty, I. H. White, and A. C. Ferrari, Int. J. Mater. Form. **1**, 107 (2008).
23. T. Hasan, Z. P. Sun, F. Q. Wang, F. Bonaccorso, P. H. Tan, A. G. Rozhin, and A. C. Ferrari, Adv. Mater. **21**, 3874 (2009).
24. S. Kivistö, T. Hakulinen, A. Kaskela, B. Aitchison, D. P. Brown, A. G. Nasibulin, E. I. Kauppinen, A. Härkönen, and O. G. Okhotnikov, Opt. Express **17**, 2358 (2009).
25. D. P. Zhou, L. Wei, B. Dong, and W. K. Liu, IEEE Photon. Technol. Lett. **22**, 9 (2010).
26. X. T. Xu, J. P. Zhai, J. S. Wang, Y. P. Chen, Y. Q. Yu, M. Zhang, I. L. Li, S. C. Ruan, and Z. K. Tang, Appl. Phys. Lett. **104**, 171107 (2014).
27. S. Xu, F. Wang, C. Zhu, Y. Meng, Y. Liu, W. Liu, J. Tang, K. Liu, G. Hu, R. C. Howe, T. Hasan, R. Zhang, Y. Shi, and Y. Xu, Nanoscale **8**, 9304 (2016).
28. R. Saito, M. Fujita, G. Dresselhaus, and M. S. Dresselhaus, Appl. Phys. Lett. **60**, 2204 (1992).
29. J.-S. Lauret, C. Voisin, G. Cassabois, C. Delalande, P. Roussignol, O. Jost, and L. Capes, Phys. Rev. Lett. **90**, 057404 (2003).
30. Y. Chen, C. Zhao, H. Huang, S. Chen, P. Tang, Z. Wang, S. Lu, H. Zhang, S. Wen, and D. Tang, J. Lightwave Technol. **31**, 2857 (2013).
31. Y. Chen, G. Jiang, S. Chen, Z. Guo, X. Yu, C. Zhao, H. Zhang, Q. Bao, S. Wen, D. Tang, and D. Fan, Opt. Express **23**, 12823 (2015).
32. Y. Huang, Z. Luo, Y. Li, M. Zhong, B. Xu, K. Che, H. Xu, Z. Cai, J. Peng, and J. Weng, Opt. Express **22**, 25258 (2014).
33. B. Dong, C. Y. Liaw, J. Z. Hao, and J. H. Hu, Appl. Opt. **49**, 5989 (2010).
34. B. Dong, J. Hu, C.-Y. Liaw, J. Z. Hao, and C. Yu, Appl. Opt. **50**, 1442 (2011).
35. J. J. Degnan, IEEE J. Quantum Electron. **31**, 1890 (1995).
36. Z. Luo, M. Zhou, J. Weng, G. Huang, H. Xu, C. Ye, and Z. Cai, Opt. Lett. **35**, 3709 (2010).
37. H. Okamoto, K. Kasuga, I. Hara, and Y. Kubota, Opt. Express **17**, 20227 (2009).